PHYSICAL REVIEW E **76**, 040903(R) (2007)

Effect of disorder on DNA electrophoresis in a microfluidic array of obstacles

Aruna Mohan and Patrick S. Doyle*
Department of Chemical Engineering, Massachusetts Institute of Technology, Cambridge, Massachusetts 02139, USA
(Received 22 August 2007; published 24 October 2007)

The size-based separation of electrophoresing DNA chains of varying lengths has been experimentally achieved in microfluidic obstacle arrays. The separation is actuated by the occurrence of size-dependent chain-obstacle collisions and the subsequent formation of hooked chain configurations in the array. We investigate the role played by disorder in array geometry in determining chain dynamics in the array. As a prototypical example of a disordered post array, we select a self-assembled array of magnetic colloids, wherein the degree of disorder may be varied by varying the magnetic field strength under which the array is generated. We employ Brownian dynamics simulations of chain electrophoresis in the array to compute the mobility, dispersivity, chain-obstacle collision probability, and mean chain stretch in the device, and demonstrate the link between the orientational order of the array and the resulting chain dynamics.

DOI: 10.1103/PhysRevE.76.040903 PACS number(s): 87.15.Tt, 87.15.He, 83.10.Mj

The efficacy of microfluidic obstacle arrays in achieving the size-based separation of DNA chains upon their motion through the array has been established in experimental studies [1–4]. Obstacle-array based separation was pioneered by Volkmuth and Austin [1], who employed optical microlithography to fabricate obstacle courses in silicon. Subsequently, Doyle *et al.* [2] and Minc and co-workers [3,4] have employed arrays comprising self-assembled columns of superparamagnetic beads confined in a microfluidic channel, formed upon the imposition of a magnetic field transverse to the channel plane. These devices rely on the application of an electric field to induce the motion of the negatively charged DNA chains through the array. The subsequent occurrence of chain-obstacle collisions and the formation of hooked chain configurations underpin the separation mechanism. The size specificity of the technique arises from the fact that a longer chain requires more time for its disengagement from an obstacle than a shorter chain, consequently taking relatively longer to traverse the array.

In a prior study on DNA electrophoretic separation in a self-assembled array of magnetic beads, the presence of disorder in the obstacle arrangement was found to be essential in effecting separation [5]. It was revealed from Brownian dynamics simulations of λ-DNA in a perfect hexagonal lattice that the chain mobility lay close to the size-independent free solution electrophoretic mobility μ_0, rapidly approaching μ_0 as the electric field strength was increased. At the same time, the dispersivity of the chain was found to be close to its free solution value. These observations indicate that a perfect lattice provides straight channels through which a chain can pass without suffering collisions. Channeling was also observed to occur in the study of Patel and Shaqfeh on chain electrophoresis in perfect square and hexagonal lattices [6]. These observations signal the need for long range disorder, which is provided by magnetic bead assemblies despite the presence of locally ordered regions therein.

Whereas Ref. [5] studied the effect of varying the electric field strength and lattice spacing on chain dynamics in a magnetic colloid assembly generated at a fixed magnetic field strength, we here investigate the effect of varying the magnetic field strength under which the array is generated and, concomitantly, the degree of array disorder. The magnetic colloid arrays are generated by means of Brownian dynamics simulation of a collection of two-dimensional hard spheres of diameter $d=1$ μm each, modeled as having repulsive point dipoles at their centers. The colloidal particles are initially placed at the lattice sites of a perfect hexagonal lattice, with the x axis chosen to lie along one of the lattice vectors. A finite magnetic field strength is applied normal to the plane of the colloidal spheres during simulation, characterized by the parameter $\Gamma=\Lambda/2(d/R)^3$, where $R=a\sin(\pi/3)$, a denotes the lattice spacing, and Λ is the ratio of the interaction potential between two dipoles oriented parallel to each other and separated by a distance d to the thermal energy k_BT [7,8]. The parameter Γ may hence be interpreted equivalently as a dimensionless interaction energy or as a dimensionless inverse temperature. We generate assemblies comprising 10 000 colloidal spheres at several values of Γ and at lattice spacings of 3 and 6 μm. A periodic unit cell of length 600.1 μm and width 129.9 μm is generated at a lattice spacing of 3 μm, while each dimension is doubled at a lattice spacing of 6 μm. The simulations are run until the defect concentration reaches steady state [8], following which the unit cell thus formed is periodically repeated to generate a semi-infinite array occupying the region $x\geqslant 0$, with the positions of the magnetic colloids being held fixed once the chain is introduced in the array. The reader is referred to Refs. [7,8] for further details of the simulation method adopted for magnetic colloid systems.

We perform Brownian dynamics simulations of the free draining, bead-spring model of YOYO-1-stained λ-DNA having a contour length of 20.5 μm in the array. The Langevin equation

$$d\mathbf{r}_j = \left(\mu_0\mathbf{E} + \frac{1}{\zeta}(\mathbf{F}_j^s + \mathbf{F}_j^{ev})\right)dt + \sqrt{\frac{2k_BT}{\zeta}}d\mathbf{W}_j \qquad (1)$$

is applied to each bead $j=1,\ldots,N$ of the chain, where $\mathbf{r}_j$ denotes the position vector of bead j relative to the origin, ζ,

*pdoyle@mit.edu

the Stokes' drag coefficient for each bead, and $\mathbf{F}_j^s$ and $\mathbf{F}_j^{ev}$ denote, respectively, the spring force exerted on bead j by the adjoining springs and the net excluded volume force exerted on bead j by the remaining beads. The distortion of the electric field $\mathbf{E}$ caused by the presence of the obstacles is neglected. The electric field and the velocity of the negatively charged DNA molecule are both measured in the positive x direction, whereby $\mu_0 > 0$. The term $\mathbf{W}_j$ represents a three-dimensional Wiener process, with $\langle d\mathbf{W}_j(t)\rangle = \mathbf{0}$ and $\langle d\mathbf{W}_j(t) d\mathbf{W}_k(t')\rangle = dt\,\delta_{jk}\delta(t-t')\boldsymbol{\delta}$, where $k=1,\ldots,N$ and $\boldsymbol{\delta}$ is the identity tensor.

We adopt the discretization used by Kim and Doyle [9] and select $N_{k,s}=5.23$ Kuhn lengths per spring, yielding a chain of $N=38$ beads, with the Kuhn length $b_k=0.106$ μm being equivalent to two persistence lengths. We quantify the electric field strength by means of the Peclet number, defined as $\mathrm{Pe}=\mu_0 E N\zeta A/(k_B T)$ with A the persistence length of ds-DNA, and perform simulations at Pe=5 and 10. We adopt the modified Marko-Siggia law [10,11] to describe the spring force-extension behavior, following Refs. [5,9]. Intrachain exclusion is modeled by means of the soft, repulsive potential developed by Jendrejack *et al.* [12], with the excluded volume parameter appearing therein taking the value $v=0.0004$ μm^3 for λ-DNA [5,9]. We adopt the semi-implicit predictor-corrector scheme [13] for the integration of Eq. (1), with a time step of 10^{-3} at Pe=5 and 5×10^{-4} at Pe=10 in units of $\zeta Q_0^2/(k_B T)$, with Q_0 the maximum spring length. Hard sphere exclusion between beads and obstacles is implemented via the Heyes-Melrose algorithm [14]. At the start of the simulation, the chain in an equilibrium coil configuration is placed upstream of the array, and is simulated in the array until the chain stretch equilibrates, fluctuating about a steady, mean value. The chain is then simulated for a further time duration before its configuration is sampled. Subsequently, the mean velocity U and dispersivity D of the chain are determined via the relations $\langle x_{cm}\rangle = Ut$ and $\mathrm{var}(x_{cm}) = 2Dt$, where t is the time duration of the simulation following the equilibration process, and x_{cm} is the x coordinate of the chain center of mass at time t. Averaging is performed over an ensemble of 1000 chains, while the mean chain stretch is determined by performing a time average after equilibration in addition to an ensemble average. We define the collision probability to be the number of chain-obstacle collisions per lattice spacing crossed by the chain center of mass, where a collision is said to have occurred when a portion of the chain is present in all four quadrants of a coordinate plane whose origin lies at the obstacle center [5]. Reference [5] contains further details of our simulation method.

Our simulation results for the velocity and dispersivity of the chain normalized with respect to their values in free solution, namely, $\mu_0 E$ and $D_0 = k_B T/(N\zeta)$, are depicted in Fig. 1, while the mean collision probability ρ and the mean chain stretch postequilibration are illustrated in Fig. 2. The occurrence of an abrupt change in all of the aforementioned chain properties at a critical value of Γ is manifestly evident in Figs. 1 and 2. In the arrays corresponding to low values of Γ, the chain is seen to undergo a number of collisions, whereby its mean velocity falls much below its value in free solution. Concomitantly, the chain possesses a highly stretched conformation on average, indicating the frequent occurrence of collisions. Similar behavior, although obscured by noise, is also exhibited by the dispersivity. Interestingly, Figs. 1 and 2 reveal the existence of a minimum in mobility and concurrently, maxima in collision probability and stretch at $\Gamma \simeq 14$. Beyond a critical value of $\Gamma = 14.89$, a steep decrease in col-

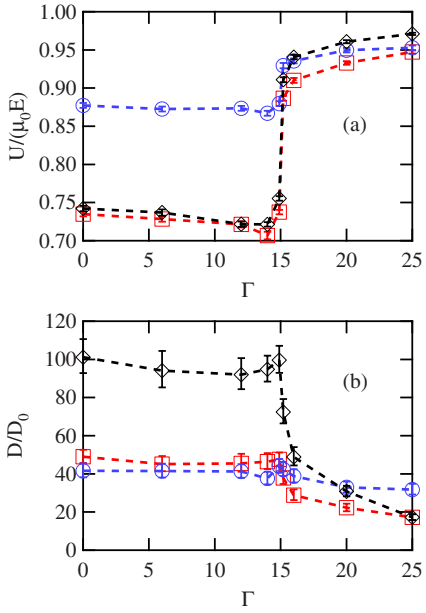

FIG. 1. (Color online) Mobility (a) and dispersivity (b) normalized with respect to their values in free solution at several values of Γ at $a=3$ μm, Pe=5 (squares), $a=6$ μm, Pe=5 (circles), and $a=3$ μm, Pe=10 (diamonds). The error bars represent 95% confidence limits. The dashed lines are meant to guide the eye.

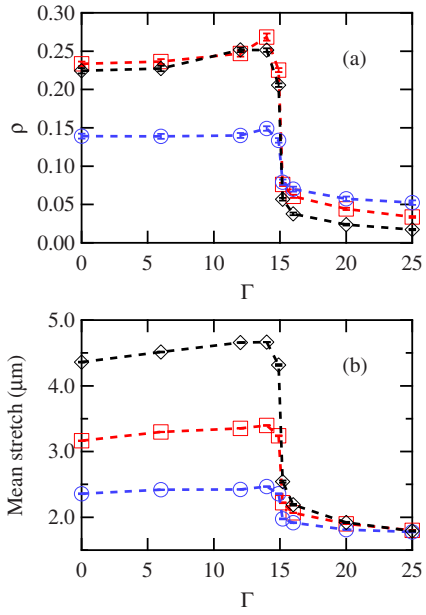

FIG. 2. (Color online) Mean probability of chain-obstacle collision ρ (a) and time-averaged chain stretch after equilibration (b) at several values of Γ at $a=3$ μm, Pe=5 (squares), $a=6$ μm, Pe=5 (circles), and $a=3$ μm, Pe=10 (diamonds). The error bars represent 95% confidence limits. The dashed lines are meant to guide the eye.

lision probability is observed, accompanied by an increase in mobility and decrease in dispersivity. The concomitant decline in mean chain stretch suggests that by and large, the chain retains its coiled conformation. These observations are indicative of the link between chain dynamics and the onset of long range order in the array at increasing values of Γ, whereby the chain is provided with channels through which it may pass without being significantly impeded by the obstacles.

The origin of the above behavior may be understood by examining the structure of the arrays at various values of Γ. Under the application of an infinite magnetic field strength transverse to the channel plane (equivalently, at zero temperature), the colloid assembly exhibits a perfect hexagonal lattice geometry. As the magnetic field strength is reduced, thermal fluctuations in the positions of the colloids result in deviations from a hexagonal pattern, culminating in a melting transition at a critical field strength. The phase transition from the solid to the liquid phase in two dimensions has been theoretically predicted to proceed via an intermediate hexatic phase [15], although evidence for the existence of a hexatic phase remains inconclusive [16]. The three phases are distinguished on the basis of orientational symmetry. The solid phase possesses long range orientational order, whereas orientational correlations decay algebraically in the proposed hexatic phase and exponentially in the liquid phase [15,16]. Orientational order may be quantified by correlations in the local order parameter $\psi_6(\mathbf{r})=\exp[6i\theta(\mathbf{r})]$, where $\theta(\mathbf{r})$ is the mean angle between the line joining nearest neighbors and an arbitrary reference axis. The corresponding correlation function is defined by the expression $G_6(\mathbf{r})=\langle\psi_6^*(\mathbf{r})\psi_6(\mathbf{0})\rangle$. In the solid phase, $G_6(r\to\infty)=\text{const}\neq 0$, signifying the presence of long range orientational order. The liquid phase exhibits the decay $G_6(r)\sim\exp[-r/\xi(T)]$, where the correlation length is of the form $\xi(T)\sim a\exp[b/(T/T_c-1)^{0.5}]$ close to the critical temperature T_c at which the liquid-hexatic transition occurs, with b a constant [15,16].

The colloidal system employed in the present study has been found to converge to the liquid phase for $\Gamma\leqslant 14.89$ and to the solid phase for $\Gamma\geqslant 15.2$ [8], an observation that we reproduced in our studies. It is now clear that the steep decline in chain-obstacle collision probability for values of Γ exceeding 14.89 is directly linked to the onset of long range orientational order in the array. The presence of orientational order is also manifest in Fig. 3, which illustrates portions of the arrays at various values of Γ, and in the behavior of $G_6(r)$ illustrated in Fig. 4. Also depicted in Fig. 4 is the pair correlation function $g(r)$ (often referred to as the radial distribution function), illustrating the increase in local order as Γ increases.

To rationalize the initial increase in collision probability for values of Γ ranging from 0 to 14, we postulate that the presence of short range orientational correlations over the length scale of the stretched DNA chain immediately following its release from a collision provides the chain with a short interstitial channel, thereby facilitating its rapid relaxation to a coil configuration and hence increasing the chain cross-sectional area subsequently presented to obstacles. Consequently, the chances of a subsequent chain-obstacle hooking collision are improved. On the other hand, a chain in a random array generated at $\Gamma=0$ (which possesses a correlation length of 0) may encounter obstacles while still in a stretched configuration immediately after its disengagement from one collision. The glancing collisions occurring as a result will likely not lead to long-lived hooking collisions, and may also delay the relaxation of the chain to a coil shape. Under the assumption that the chain relaxes instantaneously to a coil at the location of its leading end after unhooking, we postulate that the mean collision probability is maximized when $\xi\sim\mathcal{L}$, with $\mathcal{L}$ the chain extension immediately after unhooking from the obstacle. Upon coarse-graining and fitting $G_6(r)$ to an exponentially decaying form within a unit cell (although strictly valid only in an infinite system) via a least squares minimization technique, we determine that $\xi=7.0\pm0.7$ μm at $\Gamma=12$, and $\xi=13\pm2$ μm at $\Gamma=14$, averaged over five realizations of the arrays with $a=3$ μm, with the error estimates representing 95% confidence bounds. The correlation length diverges at the phase transition at $\Gamma\simeq 14.89$. The chain extension at Pe=5 and 10

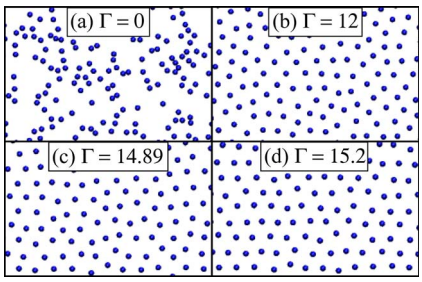

FIG. 3. (Color online) Sections of arrays having a mean lattice spacing of 3 μm generated by simulation at (a) $\Gamma=0$, (b) $\Gamma=12$, (c) $\Gamma=14.89$, and (d) $\Gamma=15.2$.

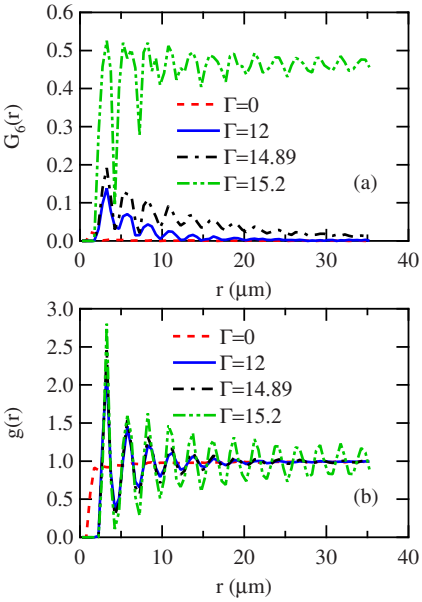

FIG. 4. (Color online) Orientational correlation function $G_6(r)$ (a) and pair correlation function $g(r)$ (b) for arrays generated by simulation at $\Gamma=0$ (dashed line), 12 (solid line), 14.89 (dashed-dotted line), and 15.2 (dashed-double-dotted line).

is determined from the large force limit of the Marko-Siggia law [5] to be 11 and 14 μm, respectively, suggesting that a maximum in the collision probability may occur close to $\Gamma = 14$. The correlation lengths are doubled at fixed Γ upon doubling a. The maximum in collision probability, however, still occurs close to $\Gamma = 14$ at $a = 6$ μm, as seen in Fig. 2. This may be attributable to the fact that the relaxation of the stretched chain subsequent to a collision does not occur instantaneously at the location of the leading chain end, but rather occurs further downstream after a finite time duration. Further studies involving a wide range of chain sizes are necessary to confirm the preceding hypotheses.

Figures 1 and 2 indicate the effect of varying Pe or a on chain dynamics. An increase in Pe restricts the ability of the chain to diffuse transverse to the electric field direction, with a concomitant reduction in collision probability, particularly in the arrays in the ordered solid phase. The dispersivity increases noticeably with increase in Pe in arrays in the liquid phase, which have a high incidence of collisions. With increase in the mean lattice spacing, the difference between chain behavior in arrays in the solid phase and in the liquid phase is attenuated, the reason being that if the mean lattice spacing greatly exceeds the chain diameter, the chain may channel through the interstices, regardless of the array geometry. Although the mean pore sizes of the arrays employed in the present study exceed the chain diameter, separation between different species may be effected even in regular arrays wherein the mean pore size falls below the diameter of the larger chain [1], owing to the dependence of chain dynamics on the chain size relative to the mean lattice spacing. These issues are elaborated in Ref. [5].

In sum, we demonstrate the link between DNA electrophoresis in an obstacle array and array order. While long range orientational order leads to the channeling of the chain, the presence of short range correlations on the scale of the chain length may increase the probability of hooking collisions and hence aid size separation in the array. These observations may be utilized in the design and fabrication of obstacle courses and other disordered substrates for DNA separation.

We are grateful to Dr. Ramin Haghgooie of MGH for providing the code for generating the magnetic colloid assemblies used in this study and for helpful discussions. We acknowledge the support of NSF NIRT Grant No. CTS-0304128.

[1] W. D. Volkmuth and R. H. Austin, Nature (London) **358**, 600 (1992).
[2] P. S. Doyle, J. Bibette, A. Bancaud, and J.-L. Viovy, Science **295**, 2237 (2002).
[3] N. Minc, C. Futterer, K. D. Dorfman, A. Bancaud, C. Gosse, C. Goubault, and J.-L. Viovy, Anal. Chem. **76**, 3770 (2004).
[4] N. Minc, P. Bokov, K. B. Zeldovich, C. Futterer, J.-L. Viovy, and K. D. Dorfman, Electrophoresis **26**, 362 (2005).
[5] A. Mohan and P. S. Doyle, Macromolecules (to be published).
[6] P. D. Patel and E. S. G. Shaqfeh, J. Chem. Phys. **118**, 2941 (2003).
[7] R. Haghgooie and P. S. Doyle, Phys. Rev. E **70**, 061408 (2004).
[8] R. Haghgooie and P. S. Doyle, Phys. Rev. E **72**, 011405 (2005).
[9] J. M. Kim and P. S. Doyle, Macromolecules (to be published).
[10] J. F. Marko and E. D. Siggia, Macromolecules **28**, 8759 (1995).
[11] P. T. Underhill and P. S. Doyle, J. Non-Newtonian Fluid Mech. **122**, 3 (2004).
[12] R. M. Jendrejack, J. J. de Pablo, and M. D. Graham, J. Chem. Phys. **116**, 7752 (2002).
[13] C. C. Hsieh, L. Li, and R. G. Larson, J. Non-Newtonian Fluid Mech. **113**, 147 (2003).
[14] D. M. Heyes and J. R. Melrose, J. Non-Newtonian Fluid Mech. **46**, 1 (1993).
[15] D. R. Nelson and B. I. Halperin, Phys. Rev. B **19**, 2457 (1979).
[16] D. R. Nelson, in *Phase Transitions and Critical Phenomena*, edited by C. Domb and J. L. Lebowitz (Academic Press, London, 1983), Vol. 7.